Article ID: 1006-8775(2016) 02-0118-09

ANALYSIS OF TROPICAL CYCLONE PRECIPITATION FOR DIFFERENT INTENSITY CLASS IN NORTHWEST PACIFIC WITH TRMM DATA

LIU Zhe (刘 喆), BAI Jie (白 洁), HUANG Bing (黄 兵),
YAN Jun (严 军), ZHOU Zhu-hua (周著华), ZHANG Wen-jun (张文军)
(Institute of Aeronautical Meteorology, Beijing 100085 China)

Abstract: Combined with TRMM products and Tropical Cyclone (TC) best track data in Northwest Pacific from 1 January 2003 to 31 December 2009, a total of 118 TCs, including 336 instantaneous TC precipitation observations are established as the TRMM TC database, and the database is stratified into four intensity classes according to the standard of TC intensity adopted by China Meteorological Administration (CMA): Severe Tropical Storm (STS), Typhoon (TY), Severe Typhoon (STY) and Super Typhoon (SuperTY). For each TC snapshot, the mean rainfall distribution is computed using 10-km annuli from the TC center to a 300-km radius, then the axisymmetric component of TC rainfall is represented by the radial distribution of the azimuthal mean rain rate; the mean rain rates, rain types occurrence and contribution proportion are computed for each TC intensity class; and the mean quadrantal distribution of rain rates along TCs motion is analyzed. The result shows that: (1) TCs mean rain rates increase with their intensity classes, and their radial distributions show single-peak characteristic gradually, and furthermore, the characteristics of rain rates occurrence and contribution proportion change from dual-peak to single-peak distribution, with the peak rain rate at about 5.0 mm/h; (2) Stratiform rain dominate the rain type in the analysis zone, while convective rain mainly occurred in the eye-wall region; (3) The values of mean rain rate in each quadrant along TCs motion are close to each other, relatively, the value in the right-rear quadrant is the smallest one.

Key words: TRMM; tropical cyclone; intensity class; precipitation
CLC number: P444 **Document code:** A
doi: 10.16555/j.1006-8775.2016.02.002

1 INTRODUCTION

Freshwater flooding due to the landfall of Tropical Cyclone (TC) has become the largest threat to human lives, so it is a great challenge to predict the distribution and variation of TCs rainfall accurately. While TC track forecasts are improved continuously, quantitative precipitation forecasts of TCs have shown little skill over the last few decades, the major reason is lack of precipitation data over the open oceans to evaluate and validate numerical weather prediction model results [1]. Therefore, providing a comprehensive analysis of TC rainfall characteristics by using effective measurements will help us to understand the TCs rainfall structure better and improve the accuracy of quantitative precipitation forecasts.

In early times, the main tools for measuring TCs rainfall include ground rain gauge, rawinsonde, weather radar etc. By analyzing the rain gauge and rawinsonde data spotted in the islands, scientists learn the distribution of TCs rainfall in near real time (Miller[2]; Frank[3]), however, their measuring range is relatively small, and their sparse and point distribution poses problems of spatial interpolation and downscaling (Kubota and Wang [4]; Marzano et al.[5]). With airborne and ground weather radar, many studies have shown that each TC has different rainfall structures during its evolution (Parish et al.[6]; Marks[7]; Burpee and Black[8]; Reasor[9]), suggesting that many factors, both related to the TC dynamics and its environment, can influence the rainfall structure, what's more, weather radar can only detect special area, and limited by many factors, including high cost, low coverage and detecting uncertainly. Satellite remote sensing overcomes the shortcomings of rain gauge and weather radar, and becomes an important tool for global precipitation observation. Detecting precipitation with satellite microwave instruments can not only retain the advantage of satellite remote sensing, but also the ability of penetration, providing reliable precipitation data globally. Rodgers and Adler [10] constructed radial profiles of rainfall for 21 eastern and western Pacific TCs using satellite passive microwave imager observations, and found that TC intensification was accompanied not only by increases in the average rain rate, but also the relative contribution of the heavy rainfall. Rodgers et al.[11] analyzed the difference of TCs rainfall structure between developing and decaying stage in North Atlantic by Special Sensor Microwave Imager data, and found that the TCs rainfall distribution is re-

Received 2014-06-09; **Revised** 2016-02-08; **Accepted** 2016-04-15
Foundation item: National Nature Science Foundation of China (41205017); Pre-Research Foundation of General Equipment Department (9140A22060215JB09349)
Biography: LIU Zhe, Ph.D., primarily undertaking research on satellite remote sensing.
Corresponding author: LIU Zhe, e-mail: lewther@aliyun.com

lated with environmental factors including sea surface temperature and wind shear closely, as well as TC specific factors such as intensity and translation speed. Unfortunately, limited by the capability and low resolution of satellite instrument, the variation mechanism of TC rainfall has not been fully understood by scientists. To solve this problem, the Tropical Rainfall Measuring Mission (TRMM) satellite was launched in 1997, and the TRMM rain sensor package includes the first space-borne Precipitation Radar (PR) and a TRMM Microwave Imager (TMI), provides three-dimensional maps of TCs rainfall structure in entire region between 35°N~35°S, makes TRMM an ideal platform to monitor TCs precipitation in the tropics. Cecil et al.[12] analyzed radar reflectivity, ice scatting and lighting derived from TRMM to show that the TC inner rainband region yielded the weakest convective signatures. Lonfat et al.[1] showed that both radial and azimuthal distributions of TCs rainfall significantly varied according to basins and intensities by utilizing TMI data. Yokoyama and Takayabu [13] analyzed TCs rain characteristics with 6 years of TRMM data, according to TCs intensity classes and stages, and compared with those of the equatorial mean, especially the average stratiform rain ratio. Jiang and Zipser[14] investigated the contribution of TCs to the global precipitation with 8 seasons of TRMM data. Corbosiero et al.[15] and Chen et al.[16] analyzed the effects of vertical wind shear and storm motion on TCs rainfall asymmetries detailedly, found that the rainfall mainly occurred in the front and right side, the left-rear was relatively poor. Tao et al.[17] and Pu et al.[18] analyzed the asymmetrical distribution structure of TC precipitation and hydormeteors in TC rain cloud with TRMM data. In conclusion, TRMM has provided reliable, continuous, and accurate rain-rate estimates based on various physical algorithms over the global tropics and subtropics that have led to a greater understanding of precipitation processes and variability (Yang and Smith[19]; Yang and Smith[20]).

As we can see, TCs rainfall structures are quite complex and vary from case to case. Significant variability was found in the observed TC rainfall, which could not be fully explained by the global variability in TCs intensity and motion from basin to basin, however, previous observational studies have focused on the Atlantic basin. Being lack of long term effective TCs rainfall observation data in Northwest Pacific, it is hard to quantify the spatial distribution of TCs precipitation. In this paper, the TRMM TC database in recent 7 years in Northwest Pacific is established to analysis TCs rainfall characteristics and its asymmetry relative to TCs motion, as a function of TCs intensity class detailed, and to understand and improve the quantitative precipitation forecast in TCs.

2 DATA AND METHODS

2.1 *TRMM TC database in Northwest Pacific*

In this study, we utilize PR 2A23, 2A25 and TMI 2A12 version 6 data from the Distributed Active Archive Center of National Aeronautics and Space Administration for the period from January 2003 to December 2009, including TMI surface rainfall estimates and PR rain-detected pixels style, details of PR and TMI algorithms are given in Iguchi et al.[21] and Kummerow et al.[22] In addition, TC best track data offered by China Meteorological Administration (CMA) are used to provide TC center position and intensity.

The analysis zone includes the domain of 100° to 180°E, 0° to 40°N in Northern hemisphere, because the lowest level condition, including the unevenly distributed land, plays an important role in TCs precipitation, what's more, TMI rain algorithm may underestimate light rain over land (Kummerow et al.[23]), only observations over the ocean are considered, so it is important to map and select the TRMM snapshots before building the TRMM TC database. First of all, the TRMM orbits containing TCs are selected by matching the TRMM snapshots to linearly interpolated TC best track, then the original TC position is interpolated to the time of the most recently TRMM data according to the track and intensity information in adjacent time. However, during the course of moving at sea, the TC may accelerate or just stay when in association with other weather systems, therefore, only the snapshot with its distance less than 100 km is selected to ensure that most part of TC cloud is included in the TRMM swath. Finally, the TCs that reached severe tropical storm intensity are selected to build the TRMM TC database, including severe tropical storm (STS), Typhoon (TY), Severe Typhoon (STY) and Super Typhoon (Super TY).

After mapping and selection, the TRMM TC database is built with 369 cases of 118 TCs that happened in Northwest Pacific from 2003 to 2009 seasons, including 107 cases of STS, with a proportion of 29.0%, 122 TY cases (33.1%), 96 STY cases (26.0%) and 44 SuperTY cases (11.9%). Fig. 1a shows the distribution of TC snapshot sources. According to the TC best track data, there are 188 TCs that happened in Northwest Pacific, including 3662 occurrences in each 6h interval, the number and proportion of STS, TY, STY and SuperTY is 832 (33.9%), 891 (36.3%), 544 (22.1%) and 188 (7.7%) respectively. Therefore we can see that the proportion of TRMM TC database is close to that of TC best track data (Fig. 1b), with the mean absolute error at 4.1%, and it can represent the distribution of TC above the intensity of STS in Northwest Pacific.

2.2 *Analysis methods*

The rainfall characteristics are derived in TC-relative coordinates. We divide the TC analysis zone into annuli every 10 km around the TC center outward to the 300-km radius, and analyze the azimuthal average characteristics of various parameters for each TC intensity class, including the radial variation of precipitation, distribution of mean rain rate occurrence and contribu-

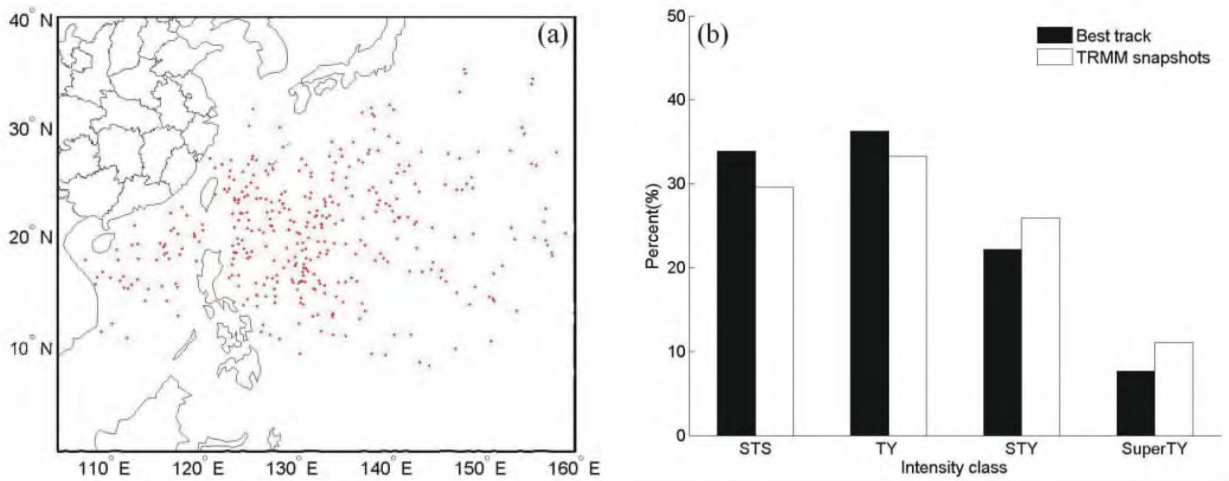

Figure 1. Distribution of the TRMM TC snapshot sources (a) and its proportion compared with TC Best track data (b).

tion proportion, radial distribution of mean stratiform, mean convective rain occurrence and contribution proportion, and the mean quadrantal distribution of rain rate according to TC motion.

Figure 2 shows the example of surface rainfall for Krosa (0716) on 5 October 2007 used in the analysis. The TC motion can then be concluded, and the first, second, third and fourth quadrant, defined based on the front-right direction of motion, is known to be distributed anticlockwise respectively.

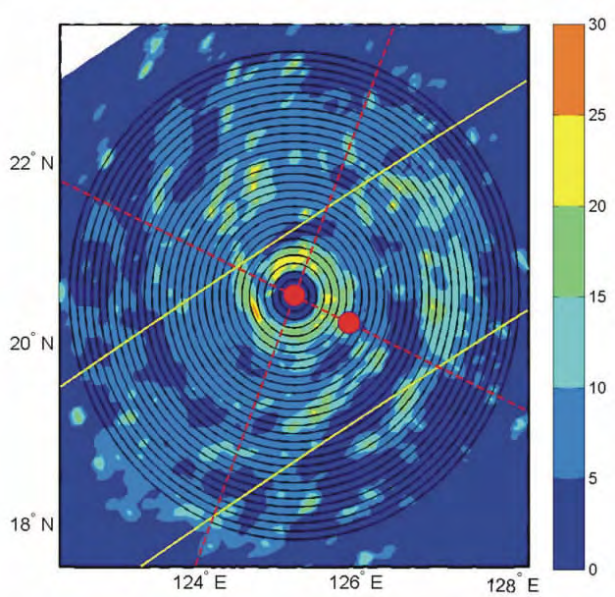

Figure 2. Example of each annuli and quadrant in this analysis (The map shows the surface rainfall of Super Typhoon Krosa on 5 October 2007 with its track number 56330). The center dot means the current TC center, the circle lines around the center indicate the 10-km wide annuli, the parallel lines which lie in the north-west and south-east of the center show the boundary of PR scanning swath, and the red dot in the south-east of the center means the TC center 6 hours before.

3 CHARACTERISTICS OF TC PRECIPITATION FOR DIFFERENT INTENSITY CLASS

3.1 *Distribution of azimuthal mean rain rates*

TC rainfall is usually composed of a ring of intense rainfall surrounding the TC center and rainbands spiraling toward the center, it differs from TC environmental factors and its dynamic developing stages. To examine how these factors affect the TC rainfall, many works have been done to study the radial distributions of TCs mean rain rates (Lonfat et al.[1]; Marks [7]; Rodgers and Adler[10]; Yokoyama and Takayabu[13]).

Figure 3a shows the mean rain rate for each TC intensity class in the TRMM TC database. As we can see, the mean rain rate of STS is 3.2 mm/h, and the value keeps increasing along with the TC intensity class, and for SuperTY, it reaches 6.9 mm/h. Fig. 3b depicts the radial profile of azimuthally averaged rain rates in each annular region for different intensity class. They are similar to each other in contour with a single-peak characteristic. For example, the existence of the eye is indicated in the TC center where the local minimum value of mean rain rate exists, and the radial distance of the peak is also found within ~50 km distance to the center. However, with the increasing of TC intensity class, its mean rain rate gets higher, and the characteristic of single-peak becomes more obvious, along with its radial distance closer to the center. As far as STS is concerned, the mean rain rate increases with radial distance, reaches the peak of 4.5 mm/h at the 60-km radii, and then decreases gradually. As to SuperTY, the peak rainfall soon reaches 11.8 mm/h at the 30-km radii and decreases rapidly. In the region outward to 200 km, their mean rain rates are close to each other. Similar to the conclusion drawn from Lonfat et al[1] and Yokoyama and Takayabu [13], the radial distribution of mean rain rates for each TC intensity class in Northwest Pacific shows a single-peak characteristic, with the radii of the maximum rainfall at about 30~50 km, and the radius of

maximum rainfall decreases with the increasing of TC intensity. Since this paper uses the TC intensity class standard defined by CMA, the exact mean rain rate value is somewhat different from previous research.

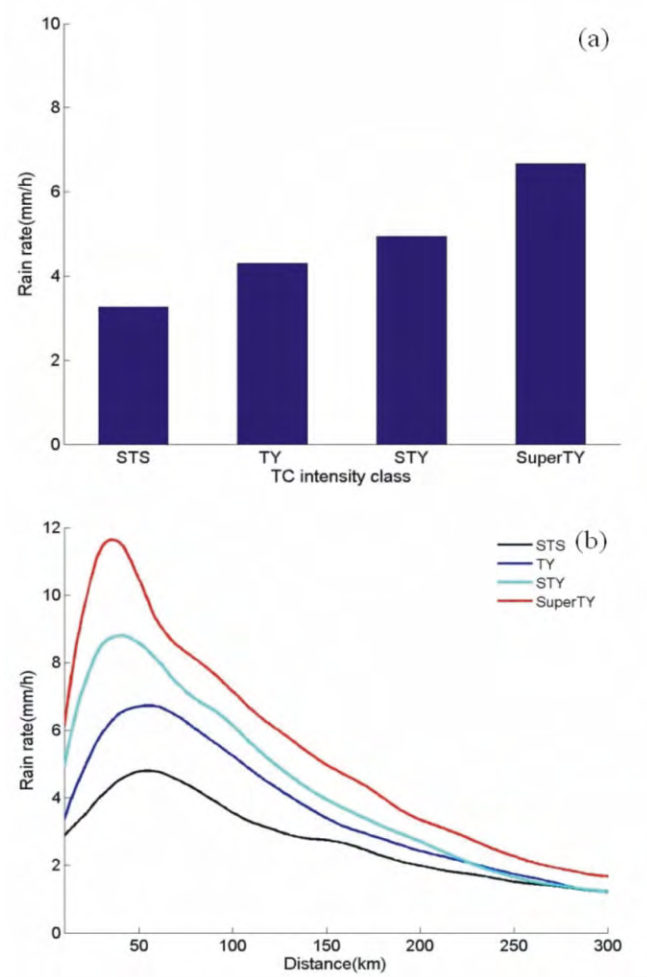

Figure 3. Mean rain rates (a) and radial profile of azimuthally averaged rain rates (b) for each TC intensity class.

Figure 4 shows the distribution of TC mean rain rates occurrence (solid line) and contribution proportion (dash line) for each TC intensity class. For convenience, a dBR scale is used to represent the rain rates, where dBR=10log10 (R), and R means rain rates. As we can see from Fig. 4a, the mean rain rates occurrence of STS shows a dual-peak characteristic, with the main and secondary peak being about 7dBR (5.0 mm/h) and -4dBR (0.4 mm/h) respectively, and the 7~13dBR rain rates produce high contribution proportion, exceeding 10%, of which the rain rate of 7dBR has not only the highest occurrence but the maximum contribution proportion. However, although the -4dBR rain rate attains 4.8% of the secondary peak of occurrence, its contribution proportion is less than 0.5% because of the relatively low rain rate. With the increasing of TC intensity class, the characteristic of occurrence changes to single-peak distribution, and the low rain rates occurrence becomes small gradually. However, the rain rates around 7dBR keep increasing with its contribution proportion. Although the characteristic of contribution proportion keeps the dual-peak distribution, the difference between the main and secondary peak becomes large. Fig. 4d shows that rain rate of SuperTY most frequently appearing around 7.3dBR (5.4 mm/h) with the contribution proportion peak of 14.2%, and the secondary peak of contribution proportion is 12.5dBR (17.8 mm/h), although its occurrence has only 3.3%.

3.2 *Distribution of different rain type*

For the rain type, TC rainfall consists of a convective regime in the eyewall and both stratiform and convective rain in the outer region, and the horizontal distribution of stratiform and convective rain has been proven to be a very useful indicator of the mesoscale structure and organization of TCs (Marks and Houze[24]). Houze [25] suggested that the large stratiform region can maintain continuous formation of convective cells, and the mesoscale convective vortices in the stratiform region could sometimes become the origin of TC circulations. Furthermore, latent heating profiles in the stratiform region are different from that of the convective region. In stratiform regions, on the other hand, it was shown that condensation heating occurred aloft and cooling was associated with the evaporation and melting below the cloud base which is found near the melting level. Therefore, the proportion of convective and stratiform precipitation can reflect the vertical heating profiles (Lin et al.[26]).

Based on the combination of a vertical profile method and a horizontal profile method described by Awaka et al. [27], rain-detected pixels are classified into stratiform, convective, or other rain type, according to PR 2A23 algorithm, and the result is consistent with that of ground and airborne-radar observations (Liang et al. [28]). Fig.5 shows the radial distribution of mean stratiform and convective rain occurrence (left side) and contribution proportion (right side) in each annuli for each TC intensity class. As we can see from Fig. 5a, the occurrence of STS stratiform rain increases with radial distance and decreases gradually after reaching the peak at the 90-km radii, and on the other hand, convective rain soon reaches the peak at the 40-km radii and then keeps fluctuating. With TCs intensification, the peak range of stratiform rain becomes larger and the peak radial distance of convective rain is observed to be closer to the center. As to SuperTY (Fig.5g), convective rain shows a single-peak characteristic obviously, and the peak value is close to that of stratiform at about the 25-km radii. Then we can see that the occurrence of TC stratiform rain is always larger than that of convective rain within the 300-km radii, and the convective rain mainly occurs near the eye-wall. The right side depicts the radial distribution of contribution proportion, and as is shown in Fig.5b, both the STS stratiform and convective rain fluctuate with radial distance, of which the latter reaches its peak at a short radius, and in the outward

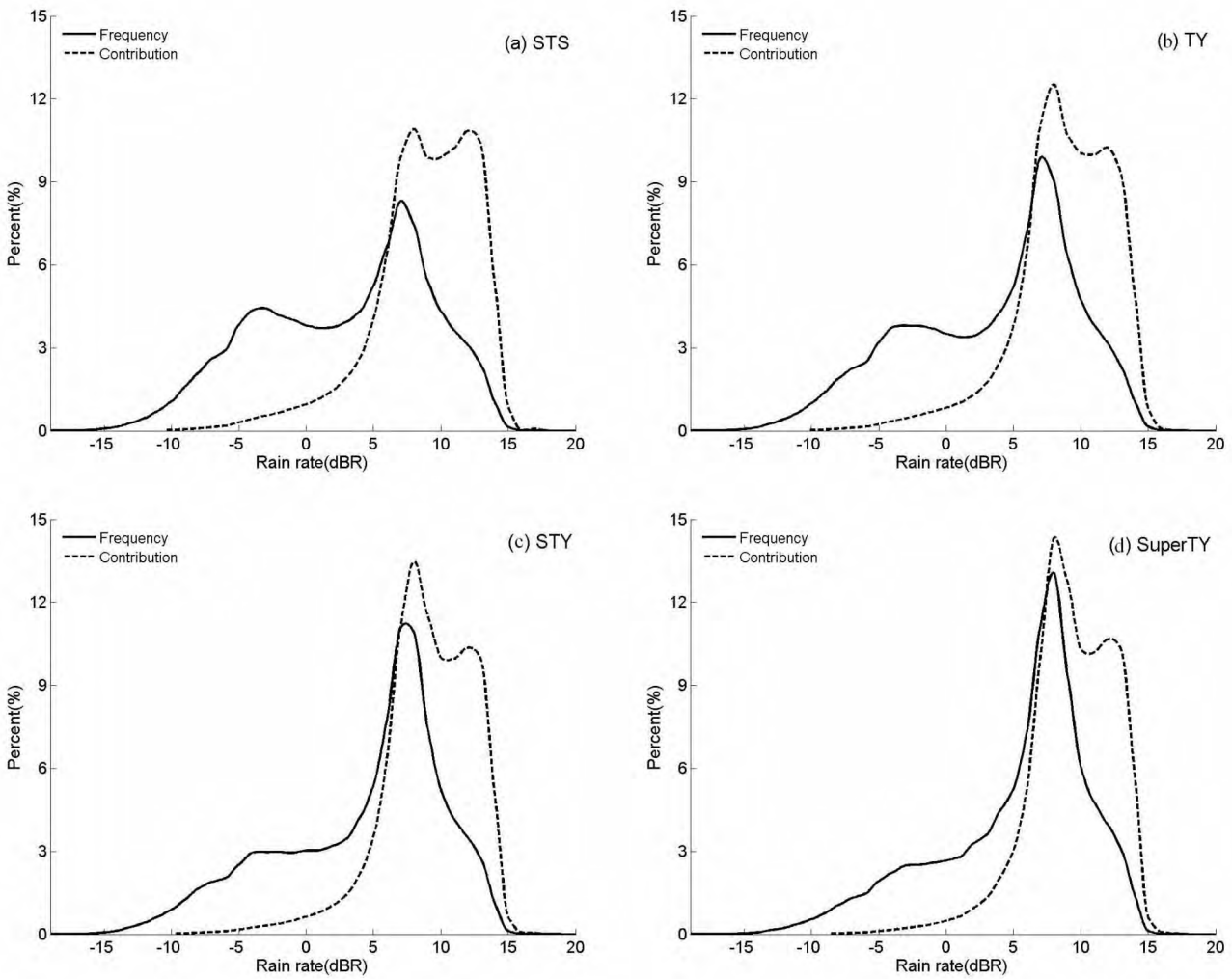

Figure 4. Distribution of mean rain rates' occurrence and contribution proportion for each TC intensity class of (a) STS, (b) TY, (c) STY, and (d) SuperTY.

area, although its occurrence is far below that of stratiform, their rain contribution proportions are close. With the increasing of intensity class, the single-peak characteristic of convective rain contribution proportion becomes more obvious, and its proportion exceeds that of stratiform gradually. For example, the peak of SuperTY convective rain reaches 60% at the 25-km radii, about 2 times stronger than the stratiform rain. Therefore we can see that the contribution proportion of convective rain exceeds the stratiform in the eye-wall area with TCs intensification and shows a single-peak characteristic obviously, but in the outer area, the stratiform rain dominates the contribution.

3.3 *Distribution of mean rain rates in each quadrant*

Influenced by many factors, including environmental factors such as planetary vorticity, wind shear, boundary layer friction, sea surface temperature, and moisture distribution, as well as specific TC factors such as intensity, location, and translation speed, the TC rainfall distribution will be asymmetrical during the course of motion. In fact, TCs with very similar locations, intensity, and speed can have very different rainfall structures (Jiang and Zipser[14]).

Many previous works have investigated TCs rainfall asymmetries with respect to environment factors and specific TC factors with varying results. Table 1 shows the research progress on quadrantal distribution of TC mean rain rates: the maximum rainfall mainly occurs in the front quadrants for the TC inner core rain-band area (r<100 km), and happens in the right quadrants for the eye-wall rain-band area (100 km<r<300 km). As the observational data resources are different, including rain gauge data, shore-based and airborne weather radar data, dropsonde observation data, space-borne microwave data, lighting detection data etc, the characteristic of TCs rainfall quadrantal distribution is somewhat complex and influenced by different measurements, data spatial resolution, TC ocean basins and TC sample cases.

This paper analyzes the influence of TCs movement on the quadrantal distribution of TC mean rain rates in the research area based on the 7-year TRMM

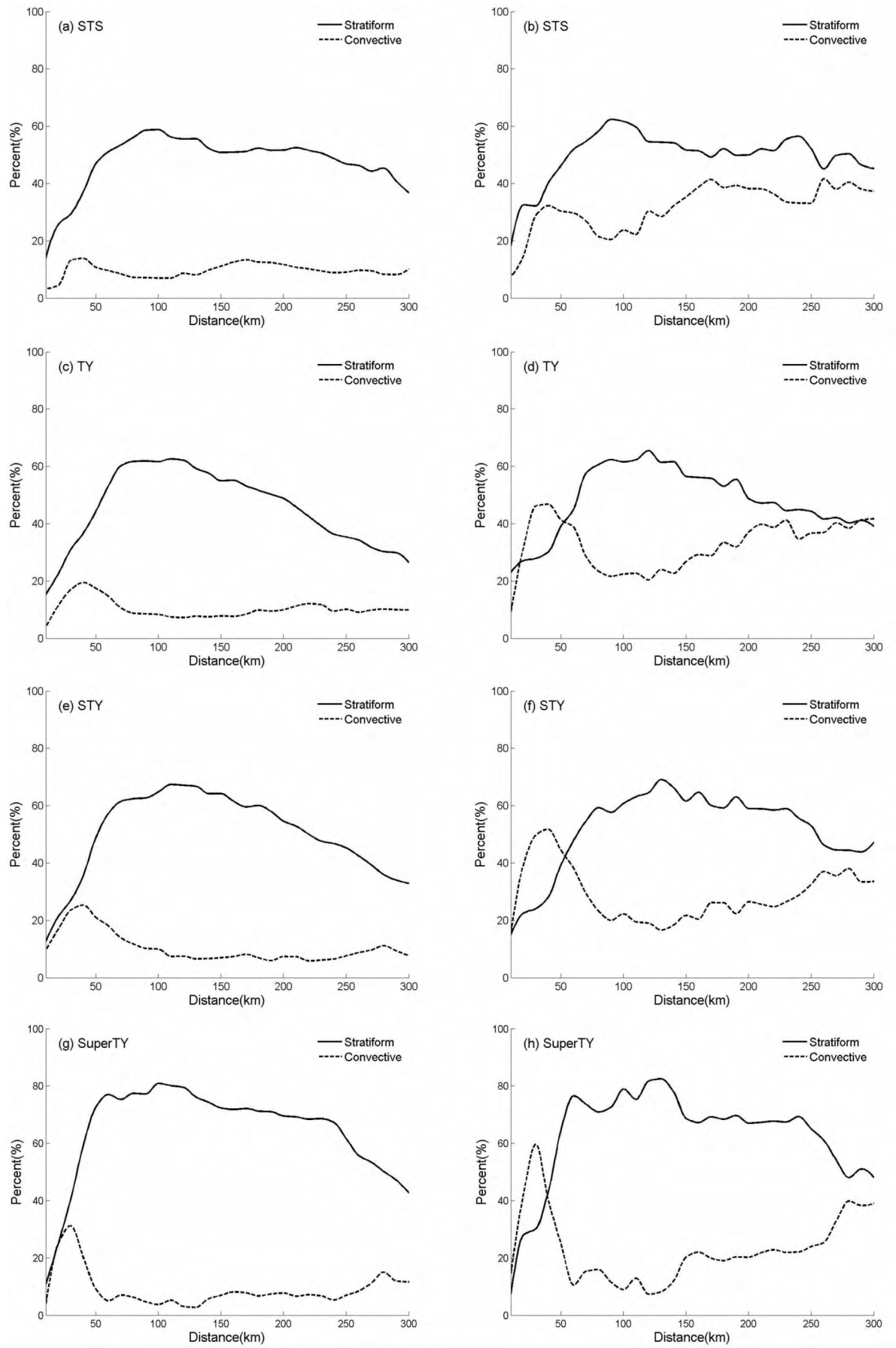

Figure 5. The radial distribution of mean stratiform and convective rain occurrence in (a), (c), (e), and (g), and contribution proportion in (b), (d), (f) and (h), for each TC intensity class.

TC database. First of all, each TC snapshot's moving direction is concluded from the current TC center and the center 6 hours before (as seen in Fig.2), then the quadrant distribution is defined anticlockwise, and finally, the mean quadrantal distribution of TCs rain rates for each intensity class is computed respectively, and the histogram chart is shown in Fig.6. As we can see that the mean rain rates increased with TCs intensification for a certain quadrant, but the extent are different, for example, the increasing amplitude from STS to TY to STY is relatively uniform in the third quadrant, about 02 mm/h, when it comes to the SuperTY class, the amplitude soon increased to 1.8 mm/h. Furthermore, TCs mean rain rates vary from quadrant to quadrant for a certain intensity class, for example, STS, TY, and STY have the maximum value in the second quadrant and minimum in the fourth quadrant, while SuperTY's maximum value lies in the third quadrant and the minimum appears in the first quadrant. The dash lines in the figure show the distribution of mean rain rates in each quadrant along TCs motion; their differences are relatively small, of which the second quadrant is the maximum one, with the value of 3.3 mm/h, followed by the third and first quadrant, leaving the fourth quadrant with the minimum. Therefore we can see that along TCs motion, the mean rain rate in the left half is larger than that of the right and the right-rear quadrant is the smallest one.

Table 1. Research progress on quadrantal distribution of TC mean rain rates[28, 29].

Author	TC cases	Research area	the Maximum rainfall
Parrish et al.[6]	Frederick(1979) in Atlantic		left-front quadrant
Willoughby et al.[29]	David(1979) and Gert(1981) in Atlantic		left-front quadrant
Marks[7]	Allen(1980) in Atlantic		right-front quadrant
Burpee and Black[8]	Alicia(1983) in Atlantic	inner core rainband r<100km	left-front quadrant
	Elena(1985) in Atlantic		right-front quadrant
Franklin et al.[30]	Gloria(1985) in Atlantic		left-front quadrant
Rodgers et al.[11]	18 TCs in North Atlantic from 1987 to 1989		front quadrants for slow-moving cases, and right quadrants for fast-moving cases
Reasor[9]	Olivia(1994) in Atlantic		left-front quadrant
Blackwell[31]	Danny(1997) in Atlantic		rear quadrant
Ueno[32]	21 TCs in Northwest Pacific in 2004		downshear-left quadrant
Miller[2]	16 TCs passing Florida USA from 1941 to 1956	eye-wall rainband 100km <r<300km	right-front quadrant
Frank[3]	248 TCs in Northwest Pacific from1961 to 1970		right-rear quadrant
Corbosiero et al.[15]	35 TCs in Atlantic from 1985 to 1999	within the research area r<300km	right-front quadrant
Lonfat et al.[1]	260 TCs all over the world from 1998 to 2000		shift from the left-front quadrant to the right-front with the increasing intensity
Chen et al.[16]	260 TCs all over the world from 1998 to 2000		downshear-left quadrant
Matthew and Daniel[33]	1131 TCs all over the world from 1988 to 2002		downshear-left (right for southern hemisphere)

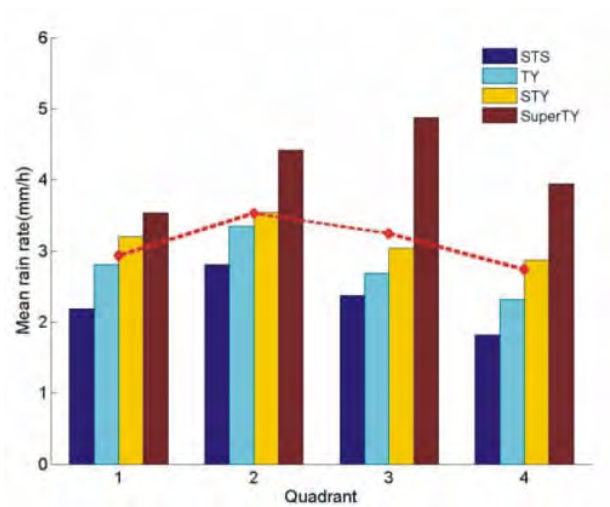

Figure 6. Mean quadrantal distribution of rain rates of TCs motion for each intensity class.

4 CONCLUSIONS

TCs precipitation distributions in Northwest Pacific have been studied using observations from the TRMM products between 1 January 2003 and 31 December 2009, and 363 instantaneous measurements were collected of 118 TCs with intensity ranging from TS to SuperTY. For each TC snapshot, the axisymmetric component of TC rainfall is represented by the radial distribution of azimuthal mean rain rate; the mean rain rates, rain types occurrence and contribution proportion are computed for each TC intensity class; and the mean quadrantal distribution of rain rates along TCs motion is analyzed.

(1) With the increasing of TCs intensity class, the radial distribution of mean rain rates shows a single-peak characteristic gradually, and the radii of the

maximum rainfall decreases.

(2) The characteristic of TCs rain rates occurrence distribution turns from dual-peak to single-peak of 7dBR with TCs intensification, along with the increasing of its contribution proportion.

(3) TCs stratiform-type rainfall dominates the occurrence distribution within the 300-km radii and its contribution proportion; the convective-type rainfall mainly occurs near the eye-wall area, and its contribution proportion exceeds that of stratiform and shows a single-peak characteristic gradually with TCs intensification.

(4) TCs mean rain rates vary with different quadrant for a certain intensity class along TCs motion relatively, and the left half is larger than that of the right and the right-rear quadrant is the smallest one.

Acknowledgement: The authors would like to thank Distributed Active Center of National Aeronautics and Space Administration for providing the TRMM data, and the China Meteorological Administration for providing the TC best track data.

REFERENCES:

[1] LONFAT M, MARKS F D, CHEN S S. Precipitation distribution in tropical cyclones using the Tropical Rainfall Measuring Mission (TRMM) microwave imager: A global perspective [J]. Mon Wea Rev, 2004, 132: 1 645-1 660.

[2] MILLER B. Rainfall rates in Florida hurricanes [J]. Mon Wea Rev, 1958, 86: 258-264.

[3] FRANK W M. The structure and energetics of the tropical cyclone I: Storm structure [J]. Mon Wea Rev, 1977, 105: 1 119-1 135.

[4] KUBOTA H, WANG B. How much do tropical cyclones affect seasonal and interannual rainfall variability over the western North Pacific? [J] J Climate, 2009, 22: 5 495-5 510.

[5] MARZANO F S, CIMINI D, MONTOPOLI M. Investigating precipitation microphysics using ground-based microwave remote sensors and disdrometer data [J]. Atmos Res, 2010, 97: 583-600.

[6] PARISH J R, BURPEE R W, Marks F D, et al. Rainfall pattern observed by digitized radar during the landfall of hurricane Frederic(1979) [J]. Mon Wea Rev, 1982, 110: 1 933-1 944.

[7] MARKS F D. Evolution of the structure of precipitation in Hurricane Allen (1980) [J]. Mon Wea Rev, 1985, 113: 909-930.

[8] BURPEE R W, BLACK M L. Temporal and spatial variations of rainfall near the centers of two tropical cyclones [J]. Mon Wea Rev, 1989, 117: 2 204-2 218.

[9] REASOR P D, MONTGOMERY M T, MARKS F D, et al. Low-wavenumber structure and evolution of the hurricane inner core observed by airborne dual-doppler radar [J]. Mon Wea Rev, 2000, 128: 506-521.

[10] RODGERS E B, ADLER R F. Tropical cyclone rainfall characteristics as determined from a satellite passive microwave radiometer [J]. Mon Wea Rev, 1981, 109: 506-521.

[11] RODGERS E B, BAIK J J, PIERCE H F. The environmental influence on tropical cyclone precipitation [J]. J Appl Meteorol, 1994, 33: 573-593.

[12] CECIL D J, ZIPSER E J, NESBITT S W. Reflectivity, ice scatting and lighting characteristics of hurricane eyewalls and rainbands. Part I: Quantitative description [J]. Mon Wea Rev, 2002, 130: 769-784.

[13] YOKOYAMA C, TAKAYABU Y N. A statistical study on rain characteristics of tropical cyclones using TRMM satellite data [J]. Mon Wea Rev, 2008, 136: 3 848-3 862.

[14] JIANG H Y, ZIPSER E J. Contribution of tropical cyclones to the global precipitation from eight seasons of TRMM data: regional, seasonal, and interannual variations [J]. J Climate, 2010, 23: 1 526-1 543.

[15] CORBOSIERO K L, MOLINARI J. The relationship between storm motion, vertical wind shear, and convective asymmetries in tropical cyclones [J]. J Atmos Sci, 2003, 60: 366-376.

[16] CHEN S S, KNAFF J A, MARKS F D. Effects of vertical wind shear and storm motion on tropical cyclone rainfall asymmetries deduced from TRMM [J]. Mon Wea Rev, 2006, 134: 3 190-3 208.

[17] TAO Li, Song YANG, LU Wei-song. 20 to 30-day and 30 to 60-day oscillations in assimilated global datasets using TRMM rainfall observations [J]. J Trop Meteorol, 2010, 16(3): 210-230.

[18] PU Jiang-ping, LV Mei, ZOU Li. An analysis of the asymmetrical structure of typhoon Aere's precipitation [J]. J Trop Meteorol, 2010, 16(1): 91-95.

[19] YANG S, SMITH E A. Mechanisms for diurnal variability of global tropical rainfall observed from TRMM [J]. J Climate, 2006, 19: 5 190-5 226.

[20] YANG S, SMITH E A. Convective-stratiform precipitation variability at seasonal scale from 8 year of TRMM observations: implications for multiple modes of diurnal variability [J]. J Climate, 2008, 21: 4 087-4 114.

[21] IGUCHI T, KOZU T, MENEGHINI R, et al. Rain-profiling algorithm for the TRMM precipitation radar [J]. J Appl Meteorol, 2000, 39: 2 038-2 052.

[22] KUMMEROW C, BARNES W, KOZU T, et al. The tropical rainfall measuring mission (TRMM) sensor package [J]. J Atmos Ocean Technol, 1998, 15: 809-817.

[23] KUMMEROW C, SIMPSON J, THIELE O, et al. The status of the tropical rainfall measuring mission (TRMM) after two years in orbit [J]. J Appl Meteorol, 2000, 39: 1 965-1 982.

[24] MARKS F D, HOUZE R A. Inner core structure of hurricane Alicia from airborne Doppler radar observations [J]. J Atmos Sci, 1987, 44: 1 296-1 317.

[25] HOUZE R A. Mesoscale convective systems [J]. Rev Geophys, 2004, 42, RG4003, doi: 10.1029/2004RG000150.

[26] LIN J L, MAPS B, ZHANG M H. Stratiform Precipitation, vertical heating profiles and the madden-julian oscillation [J]. J Atmos Sci, 2006, 61: 296-309.

[27] AWAKA J, IGUCHI T, KUMAGAI H, et al. Rain type classification algorithm for TRMM precipitation radar [C]. Proc IGARSS'97, Singapore, IEEE, 1997: 1 633-1 635.

[28] LIANG L, MENEGHINI R, IGUCHI T. Comparisons of rain rate and reflectivity factor derived from the TRMM precipitation radar and the WSR-88D over the Meibourne, Florida, site [J]. J Atmos Ocean Technol, 2001,

18(12): 1 959-1 974.
[29] WILLOUGHBY H E, JIN H L, LORD S J, et al. Hurricane structure and evolution as simulated by an axisymmetric, nonhydrostatic numerical model [J]. J Atmos Sci, 1984, 41: 1 169-1 186.
[30] FRANKLIN J L, LORD S J, FEUER S E, et al. The Kinematic Structure of Hurricane Gloria (1985) Determined from Nested Analyses of Dropwindsonde and Doppler Radar Data [J]. Mon Wea Rev, 1993, 121: 2 433-2 442.
[31] BLACKWELL K G. The Evolution of Hurricane Danny (1997) at Landfall: Doppler-Observed Eyewall Replacement, Vortex Contraction/Intensification, and Low-Level Wind Maxima [J]. Mon Wea Rev, 2000, 128: 4 002-4 016.
[32] UENO M. Observational analysis and numerical evaluation of the effects of vertical wind shear on the rainfall asymmetry in the typhoon inner-core region [J]. J Meteorol Soc Japan, 2007, 85: 115-136.
[33] MATTHEW T W, DANIEL J C. Effects of vertical wind shear on tropical cyclone precipitation [J]. Mon Wea Rev, 2010, 138: 645-662.

Citation: LIU Zhe, BAI Jie, HUANG Bing et al. Analysis of tropical cyclone precipitation for different intensity class in Northwest Pacific with TRMM data [J]. J Trop Meteorol, 2016, 22(2): 118-126.